Single-Gate Error for Superconducting Qubits Imposed by Sideband Products of IQ Mixing

Reilly P. Raab
Advisor: John Martinis

June 2015

The Thesis of Reilly Raab is Approved:

On Thu, Jun 4, 2015 at 3:09 PM, Tengiz Bibilashvili wrote:

Thank you John,

Reilly, to be formally done, please bring me printed out version with cover. You could include Professor Martinis' email as the second page in your thesis or just put his email inside your booklet.

Tengiz Bibilashvili

On Jun 4, 2015, at 1:35 PM, John Martinis wrote:

> I looked at a prior draft, and I am fine with approving it now.
>
> John
>
> On Thu, Jun 4, 2015 at 8:41 AM, Tengiz Bibilashvili wrote:
>
> > Hello John,
> >
> > Electronic approval of the final text of the thesis is as good as actual signature. So, please let me know about your opinion on the thesis.
> >
> > Reilly, please, make sure when your final draft will be approved to print it out and put it in a cover and give it to me.
> >
> > Best, Tengiz Bibilashvili
> >
> > On Jun 4, 2015, at 8:36 AM, Reilly Raab wrote:
> >
> > > Hello all,
> > >
> > > With John currently away for the next couple weeks, I'd like to crowd-source the review process for my senior thesis a bit. Granted, major overhauls aren't an option at this point, since I only have a couple of days until the due date, but if there's something worth commenting on, or if you have questions that aren't well addressed by the text, feel free to let me know.
> > >
> > > John, I think the official requirements for the thesis state that it has to be signed, but since you are away, I would imagine that emailed approval would suffice. I will be copying my adviser, Tengiz Biblilashvili, on this email.
> > >
> > > Thanks, Reilly

Professor John M. Martinis

Acknowledgements

Thank you, Sathya Guruswamy, for introducing me to the College of Creative Studies as a prospective student and for supporting such a fantastic program. I have never been inclined to think I should have studied anywhere else.

Thank you, Tengiz Bibilashvili, for playing a defining role in shaping my undergraduate experience. I have found your support for my academic success and well-being unfaltering, and I owe much of my love for CCS to you. I am extremely thankful that you worked with me to make my plans of studying abroad in Scotland a reality, and I feel that you have provided me with an agreeable balance of academic freedom and rigorous expectations.

Thank you, John Martinis, for allowing me the chance to work as a member of your lab group. I have been able to get my hands a bit dirty with a broad range of projects over the past two and a half years, and I have learned what it means to be a physicist from this lab. I admire the work ethic you promote, your focus on the overarching goals of the laboratory, and your ability to still meet my questions with interest and a friendly countenance.

To those in the Martinis lab who have helped, mentored, inspired, and welcomed me since I first joined, I thank you. It has been a tremendous benefit to have been surrounded by a wealth of knowledge that is friendly and approachable.

To my friends, especially those in the extended "Pendola(Plex)" community, you have made my time in Santa Barbara much more than a purely academic experience and I have grown significantly as a person in these last four years.

Thank you, Mom and Dad, for giving me such a rewarding life to have found myself where I am today. Dad, I thank you for my self-reliance, my love of mathematics, and my affinity for taking things apart to see how they work and putting them back together. Mom, you have worked tirelessly, and often without my full acknowledgment – probably more than I am aware – to provide me with an education which is a rare freedom and a privilege. I love you both tremendously.

To Mitchell, for keeping me on my toes about the assumptions I hold in life and for putting up with me in my ignorance. I am always proud to call you my brother.

And to Josephine, for introducing me to so many new things and for getting me to actively live and love. I have created so many memories in the past year with you that I will treasure.

Contents

Chapter 1

Introduction

This document considers the effects of non-ideal IQ mixer performance on single-qubit rotations. Some of the basic physics which supports this primary endeavor is described in the appendices. I have attempted to make this document accessible for those outside the field of quantum information, however a working knowledge of electrodynamics and quantum mechanics is assumed throughout.

The context of our discussion is the ongoing effort to build a superconducting quantum computer.

1.1 What is a Quantum Computer?

For a brief account of the history of quantum information, I could attempt no better than offered in part 1.1.1 of the book by Nielsen and Chuang.[8] For a more physical comparison between classical and quantum computation, I recommend chapter 1 of Dr. Sank's PhD thesis.[9]

Very succinctly, quantum computation is interesting because it lets us perform different types of algorithms than can be performed on a conventional computer, and some

of these algorithms solve certain problems more efficiently than any known classical method. In general, we do not know the extent of what is possible with quantum computing, as discovering useful algorithms is very difficult. We do know however that for certain cases, quantum information offers a more powerful computational paradigm than digital logic.

As of writing, no device which utilizes quantum effects has yet out-performed a classical computer, although this epoch appears imminent.

Just as a computer may be mechanical, hydraulic, or electronic, there appear to be many ways to build a quantum computer. The Martinis group works on superconducting systems. The appendices to this thesis provide an overview of the basic physics of superconducting quantum bits.

1.1.1 What is a Qubit?

The qubit (quantum bit) is the quantum analogue of the classical bit. It is the basic element that encodes information for computation. While a classical bit is strictly either a 1 or a 0 however, a qubit exists as a superposition of orthogonal states with complex amplitudes. In Dirac (bra-ket) notation, we write the qubit state

$$|\psi\rangle = c_0 |0\rangle + c_1 |1\rangle \tag{1.1}$$

We interpret $|c_0|^2$ and $|c_1|^2$ as the classical probabilities of finding the qubit in the 0 or 1 state respectively and impose the normalization condition $\langle\psi|\psi\rangle = 1$.

A qubit behaves differently than a classical bit:

- Qubits can become entangled with each other. When this happens, we can no longer treat them as superpositions of two states each. Instead, a system of n

entangled qubits is described as a superposition of the 2^n basis states formed by the tensor product of each qubit's basis states.

- It is impossible to clone a qubit's state.
- Converting a qubit to a classical bit involves a thermodynamically irreversible loss of information.

It is hard to build qubits that are useful for computation: For a qubit to have high integrity, we must isolate it from the rest of the world. To manipulate a qubit for computation, it must be coupled to a control system. The opposing nature of these criteria forms the central challenge of building a quantum computer. Useful qubit manipulations must be achieved before the quantum state is lost to decoherence caused by the interaction of the qubit with its environment.

1.2 Experimental Realization

At present, superconducting systems offer a promising, scalable architecture for the creation of a universal quantum computer.

Qubits are fabricated in a planar architecture in aluminum on a sapphire or silicon substrate using lithography techniques developed for modern CPUs and integrated circuits. The first two energy levels have a separation that corresponds to a frequency of several GHz ((B.13)).

When cooled to 20 milikelvin within a dilution refrigerator, these superconducting qubits may be manipulated with microwave frequency electronic pulses, as explained in Appendix B, which are generated by room temperature electronics and sent into the fridge through a series of filters.

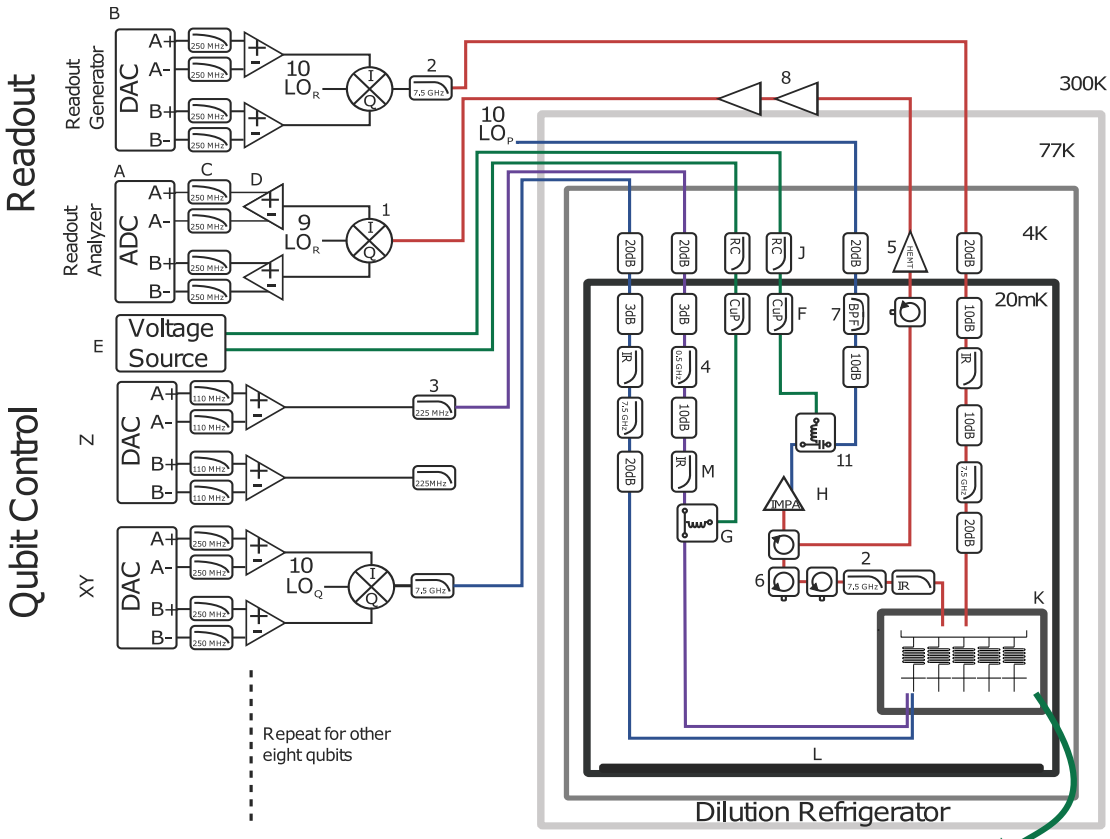

Commercial	
1	Marki IQ-0307
2	Marki FLP-0750
3	Mini Circuits VLFX-225
4	Mini Circuits VLFX-500
5	Low Noise Factory LNC4_8A
6	QuinStar CTH1392KS
7	Marki FB-1310
8	Miteq AFS3-0010200-22-10P-4
9	Hittite HMC-T2100
10	Anritsu MG3692C
11	Sigatek SB11D2

Custom	
A	Analog to Digital Converter (ADC)
B	Digital to Analog Converter (DAC)
C	Gaussian Filter
D	Differential Amplifier
E	Voltage source ("Fastbias Card")
F	Copper powder & light tight LPF
G	DC Bias T
H	Parametric Amplifier (IMPA)
J	1.5k cold resistor
K	Magnetic Shield
L	"IR-black" coating
M	Light tight LPF

Figure 1.1: Adapted diagram of a scalable architecture for manipulating superconducting qubits by Kelly et.al[3]. Used with permission. The transmon qubit pictured is described in Appendix B, although discussion of multi-qubit systems is neglected.

A key component of this approach is the use of error correcting methods such as the surface code[1] that require fast, high-fidelity qubit operations. Because these error correction methods benefit from greater qubit gate fidelity, we wish to minimize all sources of error in our control and measurement chain.

One of the room temperature devices in our control chain is the IQ mixer – pictured in the diagram above as it follows the XY Digital-to-Analog FPGA board.

Chapter 2

The IQ Mixer

The IQ mixer, also known as a quadrature mixer, is a key hardware element in the microwave chain that lets us control qubits. Although we begin with a general treatment of the device, it's use for qubit rotations is as an Image Reject (IR) or Single Sideband (SSB) mixer. Deviation from ideal performance at this element introduces error into qubit operations, and reduces gate fidelity. Thankfully, the types of errors we discuss here are easily corrected within the control software for the digital-to-analog waveform generators which generate $I(t)$ and $Q(t)$.

As a side-product of our derivations, corrections for demodulation operation of the IQ mixer will also arise.

2.1 Ideal Operation

An IQ mixer is functionally represented by two mixers and two hybrid couplers, where one coupler introduces a $\pi/2$ phase delay to one copy of a local oscillating signal. An ideal mixer (denoted by the symbol $\otimes$) multiplies two input signals, while the hybrid

couplers may be realized by conducting geometry alone to add, split, and phase-shift signals.

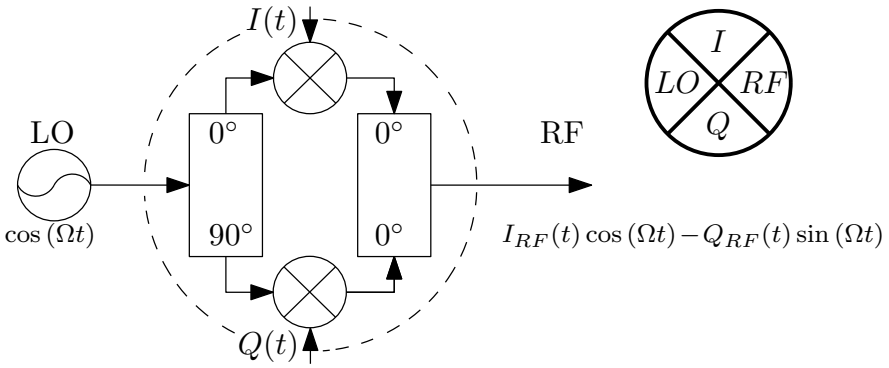

Figure 2.1: An IQ Mixer

The output of an ideal IQ mixer may be written

$$RF = I(t)\cos(\Omega t) - Q(t)\sin(\Omega t) \tag{2.1}$$

or equivalently as

$$RF = \mathrm{Re}\Big\{(I + iQ)\, e^{i\Omega t}\Big\} = \frac{1}{2}\Big[\,(I + iQ)\, e^{i\Omega t} + (I - iQ)\, e^{-i\Omega t}\Big] \tag{2.2}$$

IQ modulation may be used to mix to a single-sideband (SSB) from the LO carrier when I and Q are single-tone signals with a relative $\pi/2$ phase-shift between them:

$$\left.\begin{aligned} I &= \cos(\Delta t + \phi) \\ Q &= \sin(\Delta t + \phi) \end{aligned}\right\} \implies RF = \cos\Big((\Omega + \Delta)t + \phi\Big) \tag{2.3}$$

IQ Mixers are almost always used in this way when synthesizing signals.

2.1.1 The LO Frame

By the orthogonality of $\cos(\Omega t)$ and $\sin(\Omega t)$, we may decompose or synthesize an arbitrary time-varying signal in the basis of these two functions, where our coefficients are similarly allowed to be arbitrary functions of time:

$$f(t) = I(t)\cos(\Omega t) - Q(t)\sin(\Omega t) \tag{2.4}$$

Let us map the coefficients of this decomposition to a plane defined by the axes $\mathfrak{I}$ and $\mathfrak{Q}$. Of course, our coefficients are under-determined, as for fixed values of t, there are an infinite number of coefficients we could choose, related linearly, along a line at angle $(\pi/2 - \Omega t)$. Indeed, the contribution of any motion parallel to this line in the $\mathfrak{IQ}$ plane has no effect on the value of the synthesized or decomposed signal.

$$\begin{aligned}
&\Big(I(t) + x\cos\big(\frac{\pi}{2} - \Omega t\big)\Big)\cos(\Omega t) - \Big(Q(t) + x\sin\big(\frac{\pi}{2} - \Omega t\big)\Big)\sin(\Omega t) \\
&= \Big(I(t) + x\sin(\Omega t)\Big)\cos(\Omega t) - \Big(Q(t) + x\cos(\Omega t)\Big)\sin(\Omega t) \\
&= I(t)\cos(\Omega t) - Q(t)\sin(\Omega t)
\end{aligned} \tag{2.5}$$

This direction may be thought of as physically "imaginary".

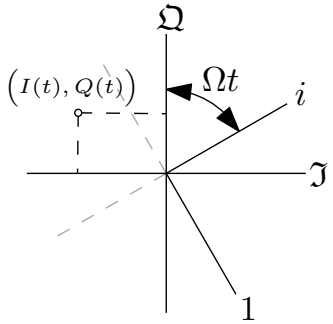

Figure 2.2: The rotating frame of the Local Oscillator in the complex plane

We think of $\mathfrak{I}$ and $\mathfrak{Q}$ axes in complex plane which rotate at angular frequency Ω according to multiplication by $e^{i\Omega t}$. In the case of the IQ mixer, we will call this the LO frame, as the angular frequency is set by the local oscillator.

We note that it is a merely a choice to have the LO frame rotate counter-clockwise: Rotation in the opposite direction is equivalent to inverting the sign of one of the axes. We choose counter-clockwise rotation by convention, but this has the consequence that any constant signal in the lab frame will rotate clockwise in the LO frame.

We also note that we are entirely capable of doing math in the LO frame by ignoring the factor of $e^{i\Omega t}$. In the LO frame, we will think of $\mathfrak{I}$ as the real axis, and $\mathfrak{Q}$ as the imaginary axis. This lets us simply map the output of an ideal IQ mixer in this frame to the point

$$\Big(I(t), Q(t)\Big) = I(t) + iQ(t) = RF_c\left(e^{-i\Omega t}\right) \tag{2.6}$$

where $I(t)$ and $Q(t)$ are the input voltages and where RF_c denotes a complex representation of the RF signal in the lab frame, with an under-determined value along the i axis.

$$RF_c = (I + iQ)\, e^{i\Omega t} \tag{2.7}$$

As in (2.2), only the real part of RF_c has any physical meaning. Due to this fact, we will allow ourselves to write

$$RF = (I + iQ)\, e^{i\Omega t} \tag{2.8}$$

for convenience, knowing that only the real part of RF is significant.

2.2 A More Realistic Model

Real IQ mixers are not perfect, and there are different ways to build a real such a device. Marki provides an overview of the doubly-double-balanced diode mixers we use.[7] In addition to introducing spurious harmonic content, these devices exhibit some non-orthogonality and amplitude imbalance between the in-phase and quadrature components of the output signal.

Let us focus on the latter errors. We will see that the end result is the introduction of an image sideband product of mixing to the qubit control. We claim that the spurious harmonic content of the mixer will introduce additional sidebands and different frequency offsets from the local oscillator. Hence, we claim that the results of our treatment for the image sideband of IQ mixing may be readily adapted to treating spurious harmonic content.

We will denote the degree of non-orthogonality in radians as δ and the degree of amplitude imbalance as ϵ. Although these parameters are in general dependent on signal frequency, LO frequency, time, or temperature, we will treat them as constant for our calculations.

Let us consider the action of the IQ mixer as a mapping of the input signals $I(t)$ and $Q(t)$ onto the LO frame given by a new set of axes:

$$RF = I(t)\mathfrak{I}' - Q(t)\mathfrak{Q}' \tag{2.9}$$

In general, these types of errors are capable of introducing overall gain and phase shifts, which equate to scaling and rotation in the LO frame. We are not concerned with either of these types of errors however: Any overall gain from the mixer will be accounted for

during the bringup routine for a qubit with unknown drive coupling [4], while an absolute phase shift is equivalent to a time delay and will have no effect on gate orthogonality.

Let us find an adequate transformation from the axes to $\mathfrak{I}$ and $\mathfrak{Q}$ to $\mathfrak{I}'$ and $\mathfrak{Q}'$ that captures this non-orthogonality and amplitude imbalance.

$$\begin{pmatrix} \mathfrak{I}' \\ \mathfrak{Q}' \end{pmatrix} = M \begin{pmatrix} \mathfrak{I} \\ \mathfrak{Q} \end{pmatrix} \tag{2.10}$$

We will do this by combining a scaling operation with two shearing operations that commute in the limit of small δ. Each operation has determinant 1 and so preserves area. To first order,

$$M = \begin{pmatrix} 1 & -\frac{\delta}{2} \\ 0 & 1 \end{pmatrix} \begin{pmatrix} 1 & 0 \\ -\frac{\delta}{2} & 1 \end{pmatrix} \begin{pmatrix} \frac{1}{\sqrt{1+\epsilon}} & 0 \\ 0 & \sqrt{1+\epsilon} \end{pmatrix} \approx \begin{pmatrix} (1-\frac{\epsilon}{2}) & -\frac{\delta}{2} \\ -\frac{\delta}{2} & (1+\frac{\epsilon}{2}) \end{pmatrix} \tag{2.11}$$

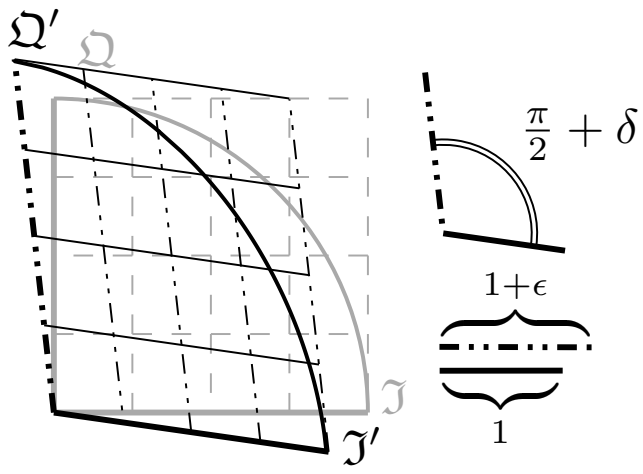

Figure 2.3: An approximately area preserving, irrotational transformation of basis vectors in the LO frame

We may express some interesting features of this transformation with the parameters s, and η which we will define by

$$s \equiv \frac{\epsilon^2 + \delta^2}{4} \quad ; \quad \eta \equiv \tan^{-1}(\frac{\delta}{\epsilon}) \tag{2.12}$$

we will see that s is equal to 1 over the sideband rejection of the mixer or the ratio of power in an image sideband to the desired signal.

The determinant of the transformation is

$$\Big|M\Big| = 1 - s \tag{2.13}$$

suggesting invertibility, while its eigendecomposition reveals orthogonal eigenvectors: Circles traced by the ideal IQ mixer are mapped to ellipses according to

$$\begin{aligned} \lambda_1 &= 1 + \sqrt{s} & \lambda_2 &= 1 - \sqrt{s} \\ \mathbf{v}_1 &= \begin{pmatrix} -\sin(\frac{\eta}{2}) \\ \cos(\frac{\eta}{2}) \end{pmatrix} & \mathbf{v}_2 &= \begin{pmatrix} \cos(\frac{\eta}{2}) \\ \sin(\frac{\eta}{2}) \end{pmatrix} \end{aligned} \tag{2.14}$$

2.2.1 Corrected Output

In accordance with (2.11), in the LO frame, we map

$$a + ib \to a - \frac{a\epsilon}{2} - \frac{b\delta}{2} + ib + i\frac{b\epsilon}{2} - i\frac{a\delta}{2} \tag{2.15}$$

from which it follows

$$e^{i\Omega t} \to e^{i\Omega t} - \frac{\epsilon + i\delta}{2} e^{-i\Omega t} \tag{2.16}$$

By applying this mapping to (2.8), the output of an IQ mixer with non-orthogonality δ and amplitude imbalance ϵ is

$$RF = \Big(I(t) + iQ(t)\Big)\left[e^{i\Omega t} - \frac{\epsilon + i\delta}{2}e^{-i\Omega t}\right] \tag{2.17}$$

or rather

$$RF = \Big(I(t) + iQ(t)\Big)\left[e^{i\Omega t} - \sqrt{s}e^{-i(\Omega t - \eta)}\right] \tag{2.18}$$

Alternately, in the limit of small δ and ϵ, we may treat the shear transformations as rotations of a single axis. Performing these operations on our model given in (2.1) directly, to first order we obtain

$$RF = I(t)\Big(1 - \frac{\epsilon}{2}\Big)\cos\Big(\Omega t + \frac{\delta}{2}\Big) - Q(t)\Big(1 + \frac{\epsilon}{2}\Big)\sin\Big(\Omega t - \frac{\delta}{2}\Big) \tag{2.19}$$

2.2.2 A Mechanical Analogue

(2.18) reveals an alternate method of construction for the ellipse mapped from the unit circle by M. Specifically, we see that the ellipse may be constructed from counter-clockwise motion along the unit circle added to a clockwise motion of radius $\sqrt{s}$ with the same angular frequency. This suggests a mechanical analog similar to epicyclic or planetary gearing:

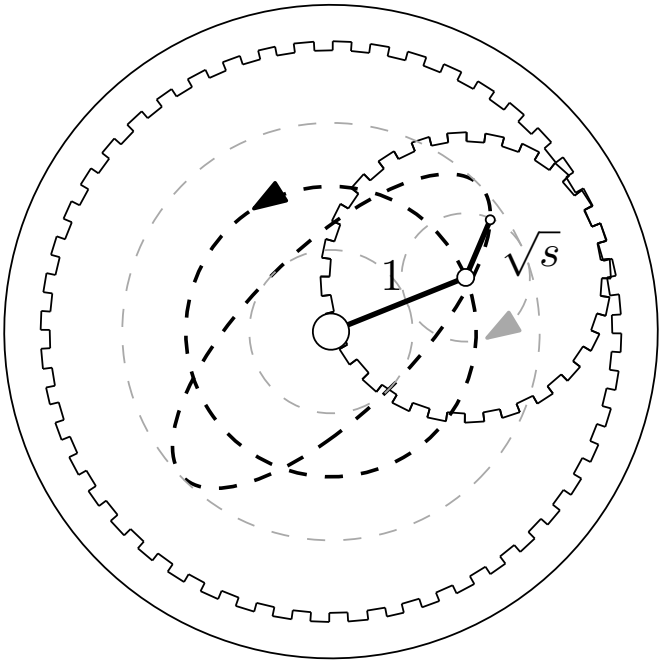

Figure 2.4: A mechanical analogue for the action of IQ mixer non-orthogonality and amplitude imbalance. In the LO frame, the outer gear is fixed. While the position of the center of the inner gear is given by (I, Q). For a pure tone of the form (2.3), the inner gear moves in a counter-clockwise path, spinning clockwise. The path traced by a point on the inner gear a distance $\sqrt{s}$ away from the center traces an ellipse.

This model is very useful for changing frames:

In the lab frame, the position of the inner gear with respect to the outer gear is given by $I(t)$ and $Q(t)$, while the outer gear spins counter-clockwise at angular frequency Ω.

To enter the qubit frame, we rotate the entire system clockwise at an angular frequency ω determined by the qubit, then walk behind the page to view it from the other side. This inconvenience is given by the differing forms of equations (2.1) and (2.23). In the qubit frame, a nominally static signal is achieved by fixing the center of the inner gear, while the outer gear rotates counterclockwise (clockwise from in front of the page) at angular frequency $\omega - \Omega$. We see that the actual signal traces circles in the qubit frame counter-clockwise (from behind the page) at angular frequency $2(\omega - \Omega)$.

We may confirm our intuition by continuing to analyze the equations.

2.2.3 Image Sideband

Equation (2.17) shows us that IQ mixer non-orthogonality and amplitude imbalance will create an image sideband during SSB mixing:

For a pure tone input signal of the form

$$I(t) = V\cos(\Delta t + \theta) \quad ; \quad Q(t) = V\sin(\Delta t + \theta) \quad ; \quad I(t) + iQ(t) = Ve^{i(\Delta t+\theta)} \tag{2.20}$$

the output of the mixer is given by

$$RF_{pt} = V\left[e^{i((\Omega+\Delta)t+\theta)} - \sqrt{s}e^{-i((\Omega-\Delta)t-\theta-\eta)}\right] \tag{2.21}$$

Or alternately

$$RF_{pt} = V\cos\Big((\Omega+\Delta)t+\theta\Big) - V\sqrt{s}\cos\Big((\Omega-\Delta)t-\theta-\eta\Big) \tag{2.22}$$

Where we observe a signal at angular frequency $(\Omega-\Delta)$ of relative amplitude $\sqrt{s}$. From this relation, we verify that s as defined in (2.12) is indeed the ratio of the power in the unwanted sideband to the desired signal, where we use the fact that for sinusoidal signals, power is proportional to the square of the amplitude in Volts.

2.3 Qubit Control

The output of the IQ mixer is coupled to a qubit with angular frequency ω. We may thus represent RF in the rotating frame of the qubit with orthogonal components X

and Y according to (B.37):

$$RF = Y(t)\cos(\omega t) - X(t)\sin(\omega t) \tag{2.23}$$

or ignoring the complex component,

$$RF = \Big(Y(t) + iX(t)\Big)e^{i(\omega t)} \tag{2.24}$$

where the voltages X and Y define an instantaneous rotation axis for a Bloch state in the rotating frame (Appendix B).

Let us appropriate the symbol Δ for the detuning of the LO from the qubit frequency, adopting a sign convention of up-mixing from the LO frequency to the higher qubit frequency:

$$\Delta \equiv \omega - \Omega \tag{2.25}$$

For the rest of this chapter, we will neglect to write the explicit time dependence of our various amplitude envelopes.

Now we consider the RF output of the IQ mixer in the rotating frame of the qubit. We first equate our different representations for the RF signal, (2.19) and (2.23), using the definition of Δ, (2.25). Introducing polar coordinates A and ϕ, we have

$$X \equiv A\cos(\phi) = -I\Big(1 - \frac{\epsilon}{2}\Big)\sin\Big(\Delta t - \frac{\delta}{2}\Big) + Q\Big(1 + \frac{\epsilon}{2}\Big)\cos\Big(\Delta t + \frac{\delta}{2}\Big) \tag{2.26}$$

$$Y \equiv A\sin(\phi) = I\Big(1 - \frac{\epsilon}{2}\Big)\cos\Big(\Delta t - \frac{\delta}{2}\Big) + Q\Big(1 + \frac{\epsilon}{2}\Big)\sin\Big(\Delta t + \frac{\delta}{2}\Big) \tag{2.27}$$

from which retrieve the law of cosines and a relation for ϕ:

$$A^2 = (1-\epsilon)I^2 + (1+\epsilon)Q^2 + 2\sin(\delta)IQ \tag{2.28}$$

$$\tan(\phi) = \frac{I\cos(\Delta t - \delta/2) + (1+\epsilon)Q\sin(\Delta t + \delta/2)}{-I\sin(\Delta t - \delta/2) + (1+\epsilon)Q\cos(\Delta t + \delta/2)} \tag{2.29}$$

Reworking the initial equations also yields

$$I = -A(1+\frac{\epsilon}{2})\sin\Big(\Delta t - \phi + \frac{\delta}{2}\Big) \tag{2.30}$$

$$Q = A(1-\frac{\epsilon}{2})\cos\Big(\Delta t - \phi - \frac{\delta}{2}\Big) \tag{2.31}$$

which we may use to send pulses to the qubit for known ϵ and δ.

2.3.1 Sideband-Induced Error

If we assume perfect IQ mixer operation when calculating the necessary I and Q for a desired amplitude A_0 and phase ϕ_0 in the rotating frame of the qubit, we let

$$I = -A_0\sin(\Delta t - \phi_0) \tag{2.32}$$

$$Q = A_0\cos(\Delta t - \phi_0) \tag{2.33}$$

Substituting these inputs into (2.28) and (2.29), our error is given to first order in δ and ϵ by Taylor expansion of the resulting expressions for A and ϕ:

$$A \approx A_0\Big[1 + \frac{\epsilon}{2}\cos\Big((2(\Delta t - \phi_0) + \xi\Big) - \frac{\delta}{2}\sin\Big(2(\Delta t - \phi_0) + \xi\Big)\Big] \tag{2.34}$$

$$\phi \approx \phi_0 + \frac{\epsilon}{2}\sin\Big(2(\Delta t - \phi_0) + \xi\Big) + \frac{\delta}{2}\cos\Big((2(\Delta t - \phi_0) + \xi\Big) \tag{2.35}$$

or rather

$$A \approx A_0\Big[1 + \sqrt{s}\cos\Big(2(\Delta t - \phi_0) + \xi + \eta\Big)\Big] \tag{2.36}$$

$$\phi \approx \phi_0 + \sqrt{s}\sin\Big(2(\Delta t - \phi_0) + \xi + \eta\Big) \tag{2.37}$$

Where we have introduced the phase ξ to account for the uncontrolled phase difference between the primary and image sidebands of mixing, or equivalently, half of the phase difference between the rotating frames of the LO and the qubit, for a gate with an arbitrary start time.

$$\xi \equiv -2\Delta t_0 \tag{2.38}$$

Unless the timing of gates is controlled with regards to the detuning frequency in a careful way, we anticipate ξ to be a quasi-linear function of the detuning and the gate time. We will treat it as being sampled from a uniform distribution.

We note that (2.34) and (2.35) agree with our mechanical model.

For reference, we compute the errors in terms of X and Y as well:

$$X \approx\ X_0\Big[1 + \sqrt{(s)}\cos\Big(2\Delta t + \xi + \eta\Big)\Big] + Y_0\Big[\sqrt{(s)}\sin\Big(2\Delta t + \xi + \eta\Big)\Big] \tag{2.39}$$

$$Y \approx\ X_0\Big[\sqrt{(s)}\sin\Big(2\Delta t + \xi + \eta\Big)\Big] + Y_0\Big[1 - \sqrt{(s)}\cos\Big(2\Delta t + \xi + \eta\Big)\Big] \tag{2.40}$$

Or in matrix form:

$$\begin{pmatrix} X - X_0 \\ Y - Y_0 \end{pmatrix} \approx \sqrt{s}\begin{pmatrix} \cos(2z) & \sin(2z) \\ \sin(2z) & -\cos(2z) \end{pmatrix}\begin{pmatrix} X_0 \\ Y_0 \end{pmatrix} \tag{2.41}$$

where $z = (\Delta t + \xi + \eta/2)$. The matrix on the right has an eigendecomposition

$$\begin{aligned} \lambda_1 &= 1 & \lambda_2 &= -1 \\ \mathbf{v}_1 &= \begin{pmatrix} \cos(z) \\ \\ \sin(z) \end{pmatrix} & \mathbf{v}_2 &= \begin{pmatrix} -\sin(z) \\ \\ \cos(z) \end{pmatrix} \end{aligned} \tag{2.42}$$

Revealing that its action is to mirror across the line defined by $\mathbf{v}_1$, which will be swept counter-clockwise with time at angular frequency Δ, tracing a circle counter-clockwise at angular frequency 2Δ with the image of a fixed point X_0 and Y_0. The vector from (X_0, Y_0) to (X, Y) traces this circle, scaled by $\sqrt{s}$, completing our analogy to the mechanical system we introduced in Section 2.2.2.

Given the way in which IQ mixer non-ideality affects qubit control, it remains to show how this translates to gate error.

Chapter 3

Quantifying Gate Errors

Having determined that the unwanted sideband product of mixing distorts our control signals to the qubit, we now wish to quantify how this affects gate error.

3.1 Single Gate Error Approximation

It is useful to derive an approximation of gate error as a function of rotation error:

Consider a rotation operation which nominally prepares a target state. Let us quantify rotation error by the distance θ_{er} on the Bloch sphere from the target state to the actual prepared state. If the target state is an eigenstate of measurement, then the probability of being measured in the target state is

$$p_t = \cos^2\left(\frac{\theta_{er}}{2}\right) \approx 1 - \frac{1}{4}\theta_{er}^2 \tag{3.1}$$

Defining gate error E in a manner consistent with randomized benchmarking[5] as $1-p_t$, we have

$$E \approx \frac{1}{4}\theta_{er}^2 \tag{3.2}$$

3.2 First Principles

We noted following (2.36) and (2.37) that we will treat ξ as being sampled from a random distribution; as such, it makes little sense to talk about η, or the relative magnitudes of ϵ and δ. We will thus focus only the relative power in the image sideband, given by s, and we will average over ξ.

The Martinis Group uses rotation pulses of duration T with a nominal Voltage envelope $A_0(t) \sim A_p \sin^2(t\pi/T)$.

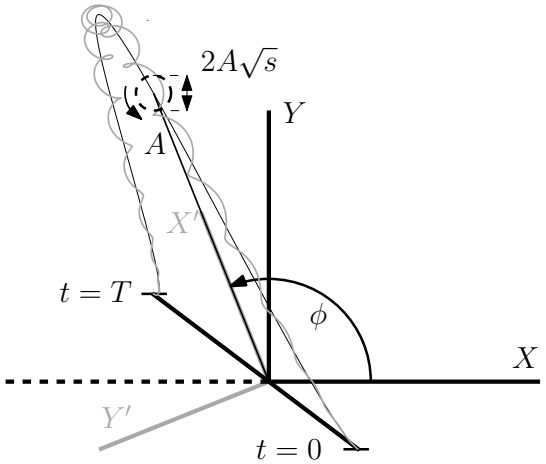

Figure 3.1: A rotation pulse with an image sideband present as seen in the rotating frame of the qubit, where depth represents time.

The rotation produced by a perfect gate is the integrated amplitude of the RF signal in the rotating frame of the qubit multiplied by $g/2\hbar$ (B.39), where g is the qubit drive

coupling given in (B.32). Requiring nominal rotations of π or $\pi/2$ radians, we may write,

$$\frac{g}{2\hbar}\int_0^T A_p \sin^2\left(\frac{t\pi}{T}\right) \mathrm{d}t = \frac{A_p T g}{4\hbar} = \Theta \quad ; \quad \Theta \in \left\{\frac{\pi}{2}, \pi\right\} \tag{3.3}$$

For generality, we will introduce two dimensionless parameters:

Let τ be the fraction of total gate time elapsed during a single gate:

$$\tau \equiv t/T \tag{3.4}$$

and let k be the wave number given by

$$k \equiv 2\Delta T \tag{3.5}$$

We may then express the accumulated rotation $\zeta(\tau)$ of a Bloch state by an ideal gate of total angle Θ as

$$\zeta(\tau) = \int_0^\tau 2\Theta \sin^2(\pi\tau')\, \mathrm{d}\tau' = 2\Theta\left(\frac{\tau}{2} - \frac{\sin(2\pi\tau)}{4\pi}\right) \tag{3.6}$$

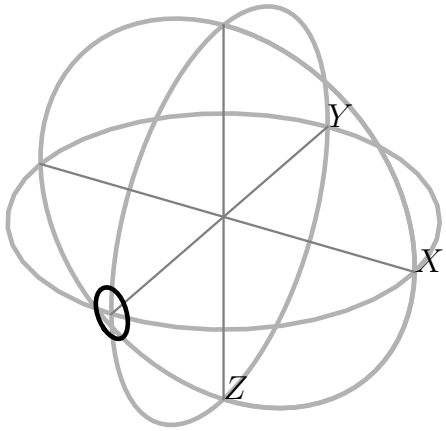

Figure 3.2: The set of final Bloch states for a simulated X($\pi/2$)-pulse starting from the ground state. The trace on the sphere represents the range of final states obtained when sweeping over the phase ξ. The expected final state is at negative Y. The wave number parameter $k = 0.32$ and the sideband rejection $s = -21.2$ dB.

We wish to predict the average distance θ on the Bloch sphere that a state prepared by an imperfect gate will be away from its target state as a function of sideband rejection and detuning so that we may use (3.2) to extract gate error. To do this, we first decompose the matrix representation of the gate $\hat{R}$ into a product of infinitesimal rotations. We will do this in a primed coordinate system that places the nominal rotation along the X' axis. Interleaved between infinitesimal $\hat{X}'$ rotations which alone would result in the nominal gate when compounded, we insert infinitesimal rotations $\hat{x}'$ and $\hat{y}'$ which represent errant rotations about the X' and Y' axes respectively due to the sideband signal.

$$\hat{R} = \prod_i \hat{x}'(\alpha_i)\hat{y}'(\beta_i)\hat{X}'(\gamma_i) \tag{3.7}$$

The degree of rotation for each matrix is allowed to vary with the index i. The product $\prod_i \hat{X}(\gamma_i)'$ will be a rotation of angle Θ, while the products $\prod_i \hat{x}'(\alpha_i)$ and $\prod_i \hat{y}'(\beta_i)$ will be smaller rotations of order θ.

We first assert that the commutators of any individual $\hat{x}'$ or $\hat{y}'$ with the total product of the matrices to the left or right will be dominated by the compounded $\hat{X}'$ rotations, as we expect rotations of order θ to approximately commute with each other. Since $[\hat{x}', \hat{X}'] = 0$, we may separate all $\hat{x}'$ operations from the rest of the product:

$$\hat{R} = \left(\prod_i \hat{x}'(\alpha_i)\right)\left(\prod_j \hat{y}'(\beta_j)\hat{X}'(\gamma_j)\right) \tag{3.8}$$

To account for the commutator of infinitesimal $\hat{y}'$ with a rotation $\hat{X}'$, we note that to first order,

$$\hat{X}'\Big(\zeta\Big)\hat{y}'\Big(\beta\Big) \approx \hat{y}'\Big(\beta\cos(\zeta)\Big)\hat{z}\Big(-\beta\sin(\zeta)\Big)\hat{X}'\Big(\zeta\Big) \tag{3.9}$$

We may approximate the commutation of $\hat{x}'$, $\hat{y}'$, and $\hat{z}$ when $\theta \ll 1$. Representing the infinitesimal degrees of rotation as functions of τ, we may now write

$$\hat{R} = \hat{x}'\left(\int_0^1 \alpha(\tau)\,\mathrm{d}\tau\right)\hat{y}'\left(\int_0^1 \beta(\tau)\cos(\zeta(\tau))\,\mathrm{d}\tau\right)\hat{z}\left(-\int_0^1 \beta(\tau)\sin(\zeta(\tau))\,\mathrm{d}\tau\right)\hat{X}'\Big(\Theta\Big) \tag{3.10}$$

where we may identify α and β with reference to (2.36) and (2.37) as oscillating signals in the rotating frame of the qubit with $\pi/2$ phase separation, frequency 2Δ, and amplitude bounded by the envelope of the gate:

$$\alpha(\tau,\xi) = 2\Theta\sqrt{s}\sin^2(\pi\tau)\cos(k\tau+\xi) \tag{3.11}$$

$$\beta(\tau,\xi) = 2\Theta\sqrt{s}\sin^2(\pi\tau)\sin(k\tau+\xi) \tag{3.12}$$

where ξ reprises its role to capture a phase dependent on time, η, and ϕ.

Let us write

$$\begin{aligned} u &= \frac{1}{2\Theta}\int_0^1 \alpha(\tau)\,\mathrm{d}\tau \\ &= \int_0^1 \sin^2(\pi\tau)\cos(k\tau+\xi)\,\mathrm{d}\tau \end{aligned} \tag{3.13}$$

$$\begin{aligned} v &= \frac{1}{2\Theta}\int_0^1 \beta(\tau)\cos(\zeta(\tau))\,\mathrm{d}\tau \\ &= \int_0^1 \sin^2(\pi\tau)\sin(k\tau+\xi)\cos\left(2\Theta\left(\frac{\tau}{2}-\frac{\sin(2\pi\tau)}{4\pi}\right)\right)\mathrm{d}\tau \end{aligned} \tag{3.14}$$

$$\begin{aligned} w &= -\frac{1}{2\Theta}\int_0^1 \beta(\tau)\sin(\zeta(\tau))\,\mathrm{d}\tau \\ &= -\int_0^1 \sin^2(\pi\tau)\sin(k\tau+\xi)\sin\left(2\Theta\left(\frac{\tau}{2}-\frac{\sin(2\pi\tau)}{4\pi}\right)\right)\mathrm{d}\tau \end{aligned} \tag{3.15}$$

and introduce the vectors

$$\mathbf{r} \equiv \begin{pmatrix} u \\ v \\ w \end{pmatrix} \quad ; \quad \boldsymbol{\psi}' \equiv \begin{pmatrix} x' \\ y' \\ z \end{pmatrix} \tag{3.16}$$

In general then, the operator for rotation error $\hat{R}\hat{X}^{\dagger}(\Theta)$ may be captured by the composition of the first three operators on the right side of equation (3.10). This composition is a rotation matrix in the three-dimensional space of the Bloch sphere, which we may represent in the basis given by the ϕ rotated axes X', Y', and Z. For small θ, we approximate this composition as a sum:

$$\hat{R}\hat{X}^{\dagger}(\Theta) = I + 2\Theta\sqrt{s} \begin{pmatrix} 0 & -w & v \\ w & 0 & -u \\ -v & u & 0 \end{pmatrix} \tag{3.17}$$

We may represent the action of $\hat{r}$ for small θ as the addition of a cross-product term. The deviation from the nominal gate $\hat{X'(\Theta)}$ is thus

$$\boldsymbol{\theta} = 2\Theta\sqrt{s}\,[\boldsymbol{\psi}' \times \mathbf{r}] \tag{3.18}$$

and we may extract the single-gate error using equation (3.2):

$$E \approx s\,||\boldsymbol{\psi}' \times \mathbf{r}||\,\Theta^2 \tag{3.19}$$

We will comment here that our results are more general than discussions about an image sideband of IQ mixing: If the relative phase shift and power of each harmonic is known for spurious frequencies produced by the IQ mixer, the mathematics we have developed in this section may be applied. These results are also applicable to systems in which multiple frequency-addressed qubits share a single drive line: In this case, we allow Θ to be values other than $\pi/2$ or π.

3.2.1 Bounding Average Gate Error

As a vector cross-product, E is easily maximized for normalized $\boldsymbol{\psi}$:

$$E_{max} \approx s\left(u^2 + v^2 + w^2\right)\Theta^2 \tag{3.20}$$

Let us consider gate error averaged over ξ. In this average, v^2 and w^2 are equivalent. This may be shown by rewriting the integrals by appeal to (3.6) and (3.12):

$$v = \int_0^\Theta \sqrt{s}\cos\left(\zeta\right)\sin\left(k\tau(\zeta) + \xi\right)\mathrm{d}\zeta \tag{3.21}$$

$$w = -\int_0^\Theta \sqrt{s}\sin\left(\zeta\right)\sin\left(k\tau(\zeta) + \xi\right)\mathrm{d}\zeta \tag{3.22}$$

As an aside, we comment that $\tau(\zeta)$ has no algebraic solution; (3.6) has a functional form equivalent to Kepler's Equation with eccentricity 1. As such, we should not expect to be able to do these integrals by hand.

We may thus bound average gate error due to the presence of a sideband on the qubit drive channel:

$$\langle E_{max}\rangle_\xi \approx s\left(\left\langle u^2\right\rangle_\xi + 2\left\langle v^2\right\rangle_\xi\right)\Theta^2 \tag{3.23}$$

where we use angle brackets with a subscript ξ to denote an average over that variable.

Let us evaluate this result.

We start with u^2:

$$u = \int_0^1 \sin^2(\pi\tau)\cos(k\tau + \xi)\,\mathrm{d}\tau = \frac{\cos\left(\frac{k}{2} + \xi\right)\sin\left(\frac{k}{2}\right)}{k\left(1 - \frac{k^2}{(2\pi)^2}\right)} \tag{3.24}$$

When squared and averaged over ξ, we may replace the factor of $\cos^2$ with $1/2$ to obtain

$$\left\langle u^2 \right\rangle_\xi = \frac{\sin^2\left(\frac{k}{2}\right)}{2k^2\left(1-\frac{k^2}{(2\pi)^2}\right)^2} \tag{3.25}$$

As we noted above, we should not expect to be able to compute $\langle v^2 \rangle_\xi$ by hand. We shall write down the expression:

$$\left\langle v^2 \right\rangle_\xi = \frac{1}{\pi}\int_0^\pi \mathrm{d}\xi \left(\int_0^1 \mathrm{d}\tau \cos\left(2\Theta\Big(\frac{\tau}{2} - \frac{\sin\left(2\pi\tau\right)}{4\pi}\Big)\right)\sin^2\left(\pi\tau\right)\sin\Big(k\tau+\xi\Big)\right)^2 \tag{3.26}$$

As consolation, we can at least compute the value of $\langle E_{max} \rangle_\xi$ when $k = 0$:

$$\langle E_{max}\rangle_\xi \Big|_{k=0} = s\frac{\Theta^2}{8} + \frac{s\sin^2\left(\Theta\right)}{4} \tag{3.27}$$

We will resort to a graphical representation of our full results, obtained numerically, for π and $\pi/2$ gates:

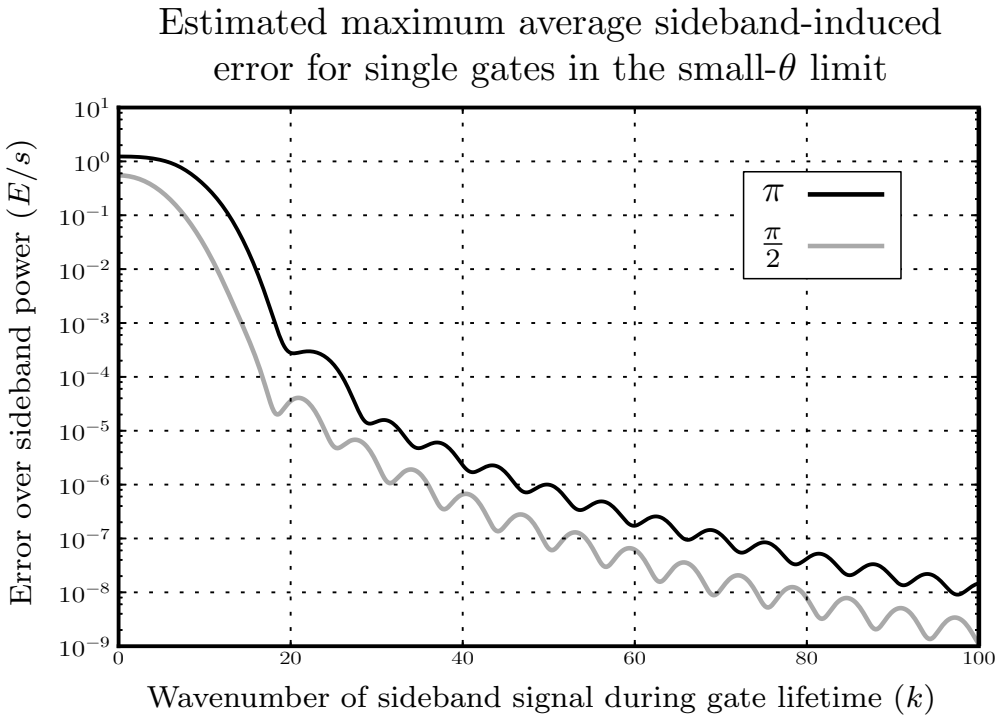

Figure 3.3: Estimated maximum average gate error $\langle E_{max} \rangle_{\xi}$ for $\pi/2$ and π rotations normalized by the power s in the image sideband. The x-axis value k corresponds to a wave-number – the product of the angular frequency of detuning between the qubit and the image sideband and the gate time T. For a constant k, we expect gate error E to be directly proportional to the sideband rejection s.

In general, we note that the errors due to π rotations are an order of magnitude greater than those for $\pi/2$ gates. We anticipate that the total error rate due to the presence of image sidebands will depend on the ratio of π gates to $\pi/2$ gates used in any given algorithm.

3.3 Simulation

To evaluate our approximations, let us assume the types of IQ mixer errors we have discussed and apply them to the control of simulated qubits, integrating the equations of motion. This simulation uses a nice chunk of the Martinis group code base which

was modified slightly to accommodate this error mechanism. The list of contributors is sizable.

We will simulate π and $\pi/2$ gates starting from the ground state, averaging over ξ. Because u, v, and w are all dependent on ξ, even if we happen upon the lucky scenario that places our final state on the vector $\mathbf{r}$ and eliminates our sideband error for one data point, we this to be drowned out by all other data points.

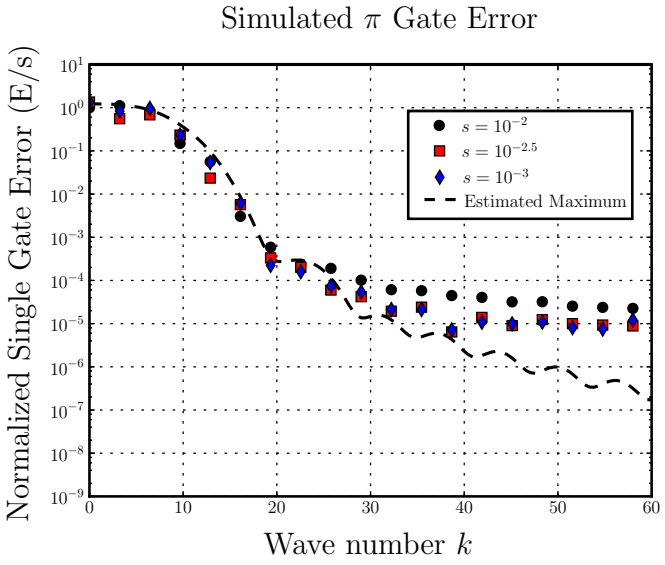

Figure 3.4: Simulated gate error for π-gates normalized by s, averaged over 10 evenly spaced, but randomly oriented samples of ξ. Different values of s were simulated. The dashed line represents the small-s limit calculated above.

Unfortunately, we have a noise floor to the simulation of $\sim 10^{-8}$, as errors of this magnitude are present even when $s = 0$. While our predictions appear to hold up well above this noise floor, increasing s to maximize visibility of the high-detuning behavior begins to violate the assumptions of our model, which was taken in the limit of small s. We thus have a limited dynamic range in which we are able to evaluate our model.

It appears that values of s in the neighborhood of $10^{-2.5}$ is the best that we are able to do, yet for a noise floor $\sim 10^{-4.5}$ below that, our model still agrees quite well.

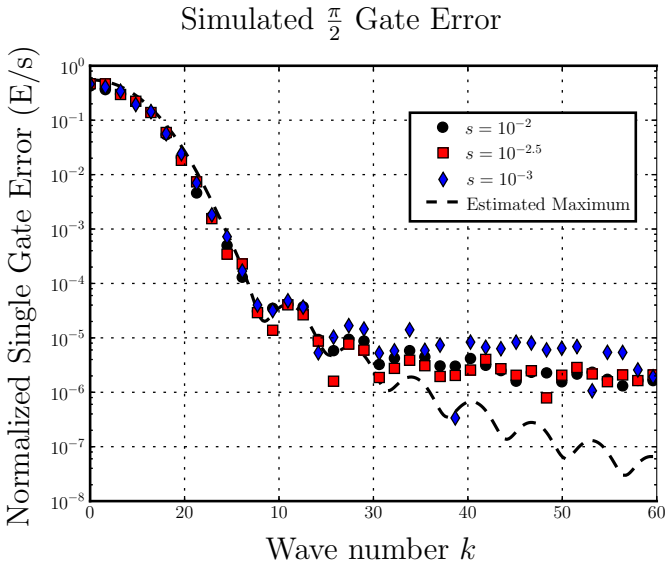

Figure 3.5: A repeated simulation of single-gate error for $\pi/2$-gates.

In addition to partially verifying our predictions of Gate Error as a function of detuning, we may also confirm the linear scaling of the gate error with sideband power. The noise floor of the simulation again becomes apparent at $\sim 10^{-8}$.

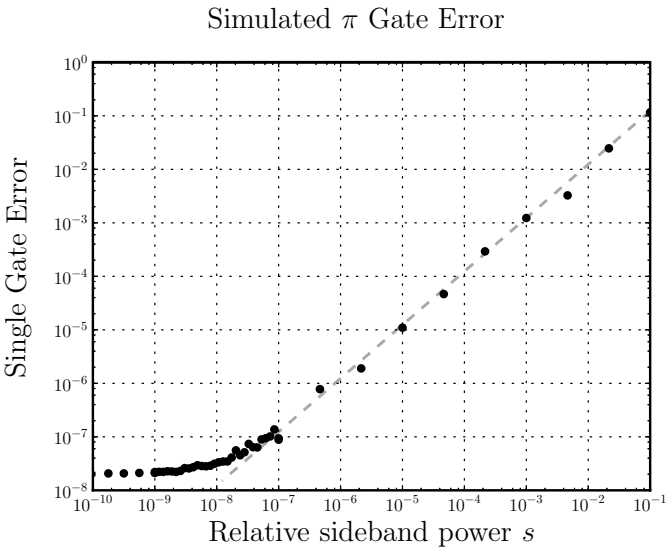

Figure 3.6: Simulated gate error for π-gates at zero detuning, with varied sideband power s. The dashed lines represent the predictions given by equation (3.27).

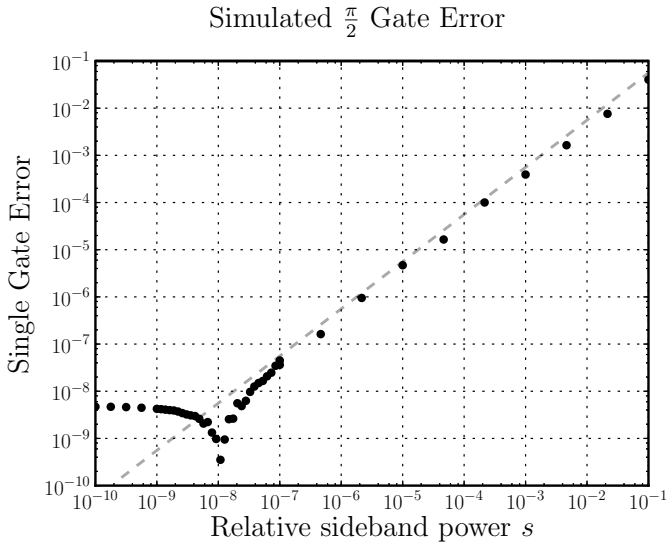

Figure 3.7: A repeated simulation for $\pi/2$-gates. The notch at 10^{-8} is curious, although an explanation was not immediately forthcoming. (3.27).

Without time to write a new simulation package, and without the knowledge to increase the accuracy of the existing software, we will fly our "Mission Accomplished" banner and conclude the exposition of this thesis. Thank you sincerely for your attention.

Appendix A

Superconductivity

Let us briefly derive the equations that govern Josephson junctions and SQUID loops as they pertain to superconducting qubits. A formal treatment of superconductivity from thermodynamic considerations will be unnecessary, though we will gloss over our definition of critical current. We will use the wave-function of a condensate of Cooper pairs in conjunction with a classical Hamiltonian to derive the phase-current and phase-Voltage relations for a single Josephson junction before analyzing SQUID loops. More rigorous derivations are presented by Martinis and Osborne. [2]

For some expressions, we will implicitly substitute the flux quantum Φ_0, which is justified in A.3.1.

$$\frac{2\pi}{\Phi_0} \equiv \frac{2e}{\hbar}$$

A.1 Semiclassical Tools

A.1.1 Probability Current

We begin with a quantum mechanical description of current. Given a macroscopic wave function ψ that describes a Bose-Einstein condensate of Cooper pairs, we appeal to the classical Hamiltonian for a charged particle without magnetic moment in an Electromagnetic field:

$$\hat{H} = \frac{1}{2m}(\hat{\mathbf{p}} - q\mathbf{A})^2 + qV \tag{A.1}$$

We should clarify that the normalization condition on ψ should correspond to a single charged particle, thus the magnitude of $\int d^3r|\psi|^2$ corresponds to the number of charged particles contained within the integrated region. The magnitude of $|\psi|^2$ thus corresponds to classical number density.

We begin by writing down the momentum operator and the time-dependent Schrödinger equation for reference

$$\hat{\mathbf{p}} = -i\hbar\nabla \tag{A.2}$$

$$i\hbar\partial_t = \hat{H} \tag{A.3}$$

Applying the Schrödinger equation to ψ, we obtain

$$\begin{aligned} \partial_t\psi &= \frac{-i}{\hbar}\left(\frac{1}{2m}(i\hbar\nabla + q\mathbf{A})^2 + qV\right)\psi \\ \implies \partial_t\psi^* &= \frac{i}{\hbar}\left(\frac{1}{2m}(i\hbar\nabla - q\mathbf{A})^2 + qV\right)\psi^* \end{aligned} \tag{A.4}$$

Identifying $\psi^*\psi$ as particle number density and taking a time derivative, (A.4) and its complex conjugate find direct substitution via the product rule:

$$\partial_t(\psi^*\psi) = \psi^*\frac{-i}{\hbar}\left(\frac{1}{2m}(i\hbar\nabla + q\mathbf{A})^2 + qV\right)\psi + \psi\frac{i}{\hbar}\left(\frac{1}{2m}(i\hbar\nabla - q\mathbf{A})^2 + qV\right)\psi^*$$

We note that terms of V and A^2 cancel and drop out of the expression. We next expand one cross term from each binomial according to the vector identity

$$\nabla(\mathbf{A}\psi) = (\nabla\cdot\mathbf{A})\psi + \mathbf{A}\cdot(\nabla\psi) \tag{A.5}$$

to obtain

$$\partial_t(\psi^*\psi) = \frac{i\hbar}{2m}\left[\psi^*\nabla^2\psi - \psi\nabla^2\psi^*\right] + \frac{q}{m}\left[\psi^*\mathbf{A}\cdot\nabla\psi + \psi\mathbf{A}\cdot\nabla\psi^* + (\nabla\cdot\mathbf{A})\psi^*\psi\right]$$

Utilizing the vector identities

$$\psi^*\nabla^2\psi = \nabla(\psi^*\nabla\psi) - (\nabla\psi^*)(\nabla\psi) \tag{A.6}$$

$$\psi^*\mathbf{A}\cdot\nabla\psi + \psi\mathbf{A}\cdot\nabla\psi^* + (\nabla\cdot\mathbf{A})\psi^*\psi = \nabla(\mathbf{A}\psi^*\psi) \tag{A.7}$$

We see that

$$\partial_t(\psi^*\psi) = \nabla\cdot\left[\frac{i\hbar}{2m}(\psi^*\nabla\psi - \psi\nabla\psi^*) + \frac{q}{m}\mathbf{A}\psi^*\psi\right] \tag{A.8}$$

But we may define the probability current $\mathbf{j}$ by the continuity equation,

$$\partial_t(\psi^*\psi) \equiv -\nabla\cdot\mathbf{j} \tag{A.9}$$

where $\mathbf{j}$ has units of $[s]^{-1}[m]^{-2}$. Hence

$$\mathbf{j} = \frac{\hbar}{2im}(\psi^*\nabla\psi - \psi\nabla\psi^*) - \frac{q}{m}\mathbf{A}|\psi|^2 \tag{A.10}$$

Before continuing, we will find it convenient to present an alternate form of this equation. Noting that

$$\begin{aligned}\mathbf{j} &= \frac{\hbar}{2m}[(-i\psi^*)(\nabla\psi) + (i\psi)(\nabla\psi^*)] - \frac{q}{m}\mathbf{A}|\psi|^2 \\ &= \mathrm{Re}\left\{-\psi^*\frac{1}{m}(i\hbar\nabla + q\mathbf{A})\psi\right\}\end{aligned} \tag{A.11}$$

If we write the form of ψ as a product of amplitude and phase,

$$\psi = |\psi|e^{i\theta} \tag{A.12}$$

We may substitute (A.12) into (A.11) to write the probability current as

$$\mathbf{j} = |\psi|^2\frac{1}{m}(\hbar\nabla\theta - q\mathbf{A}) \tag{A.13}$$

A.1.2 Conventional Current in a Superconductor

Conventional current density $\mathbf{J}$ is given by

$$\mathbf{J} \equiv q\mathbf{j} \tag{A.14}$$

We may write conventional current in the forms of (A.10) and (A.13), where we will substitute $m_{cp} \approx 2m_e$ for the mass of a Cooper pair with charge $q_{cp} = -2e$.

$$\mathbf{J} = \frac{ie\hbar}{m_{cp}}(\psi^*\nabla\psi - \psi\nabla\psi^*) - \frac{4e^2}{m_{cp}}\mathbf{A}|\psi|^2 \tag{A.15}$$

$$\mathbf{J} = -\frac{2e|\psi|^2}{m_{cp}}(\hbar\nabla\theta + 2e\mathbf{A}) \tag{A.16}$$

A.1.3 Gauge Invariant Phase Differences

We have not yet limited ourselves to a particular gauge choice in deriving our expressions for probability current or conventional current. Given that $\mathbf{J}$ is observable and thus gauge independent, it is apparent that θ must respond to gauge transformations of $\mathbf{A}$. Specifically, we are constrained by (A.16) to demand

$$\mathbf{A}' = \mathbf{A} + \nabla\chi \iff \theta' = \theta - \frac{2e}{\hbar}\chi \tag{A.17}$$

We wish to define differences of phase which will be gauge invariant. In general however, the vector field $\nabla\chi$ need not be constant; performing a gauge transformation according to (A.17) leaves the simple definition of phase difference $\theta_b - \theta_a$ gauge dependent. To amend our definition to this constraint, we will define the gauge invariant phase difference δ between points a and b according to the equation

$$\delta \equiv \theta_b - \theta_a + \frac{2e}{\hbar}\int_a^b \mathbf{A}\cdot d\mathbf{l} \tag{A.18}$$

A.2 Josephson Junctions

Josephson Junctions are realized by two superconducting regions separated by a thin insulator. The insulator is thin enough to allow the tunneling of Cooper pairs across the junction.

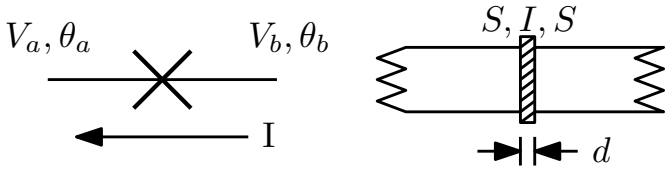

Figure A.1: Two Depictions of a Josephson Junction

A.2.1 Current-Phase Relation

A common derivation of the Current-Phase Relation may be obtained by the standard treatment of tunneling across as potential barrier: It involves solving Schrödinger's equation in three regions of space and joining the solutions by matching boundary conditions. We present an alternative derivation which assumes a finite phase difference across an infinitesimal distance in an otherwise superconducting bulk.

Consider two superconducting regions separated by a thin region of thickness d in the x direction (figure A.1). With sufficient smallness of d, we may approximate

$$\nabla\psi = \partial_x\psi \approx \frac{\psi_b - \psi_a}{d}$$

where we have chosen the vector from point a to point b to be the positive x-axis.

For simplicity, let us choose the Coulomb gauge ($\nabla \cdot \mathbf{A} = 0$). Noting the expulsion of magnetic fields from a superconducting bulk via the Meissner effect, ($\mathbf{B} = \nabla \times \mathbf{A} = 0$), we may appeal to Helmholtz decomposition to set $\mathbf{A} = 0$ in the presence of weak magnetic fields. This has the added consequence of setting $\delta = \theta_b - \theta_a$.

Substituting our approximation into (A.15), we see

$$\mathbf{J}_x = \frac{ie\hbar}{m_{cp}}\left[{\psi_a}^*\frac{\psi_b - \psi_a}{d} - \psi_a\frac{{\psi_b}^* - {\psi_a}^*}{d}\right]$$

Writing the wave function on either side of the junction as a product of amplitude and phase (A.12), this evaluates to

$$\mathbf{J}_x = -\frac{2e\hbar|\psi_a||\psi_b|}{m_{cp}d}\Big[\frac{e^{i(\theta_b-\theta_a)} - e^{-i(\theta_b-\theta_a)}}{2i}\Big] \tag{A.19}$$

Choosing to define the positive direction of current to be from b to a so as to be consistent with Ohm's law – $\mathrm{sgn}\,(I) = \mathrm{sgn}\,(V_b - V_a)$ – we write.

$$\mathbf{J}_{\leftarrow} = \frac{2e\hbar|\psi_a||\psi_b|}{m_{cp}d}\sin(\delta)$$

Identifying the coefficient of sin as the critical current density of the junction (by which an unbiased supercurrent is bounded without regard to phase), we arrive at the Josephson current-phase relation:

$$I = I_c \sin(\delta) \tag{A.20}$$

A.2.2 Voltage-Phase Relation

Appealing to the Meissner effect in a bulk superconductor, the Lorentz force reduces to

$$\mathbf{F} = q[\mathbf{E} + (\mathbf{v} \times \mathbf{B})] = q\mathbf{E} \tag{A.21}$$

By Newton's second law, we then have

$$q\mathbf{E} = m\frac{\partial_t \mathbf{j}}{|\psi|^2} \tag{A.22}$$

where we interpret $\mathbf{j}$ as classical particle velocity density $\mathbf{j} = |\psi|^2\mathbf{v}$. Expanding $\mathbf{j}$ according to (A.13), we have

$$\mathbf{E} = -\frac{\hbar}{2e}\frac{\partial}{\partial t}(\nabla\theta + \frac{2e}{\hbar}\mathbf{A}) \tag{A.23}$$

Integrating across the junction yields

$$\Delta V = \frac{\hbar}{2e}\frac{\partial}{\partial t}\left[\theta_b - \theta_a + \frac{2e}{\hbar}\int_a^b \mathbf{A}\cdot d\mathbf{l}\right] \tag{A.24}$$

Substituting our definition for phase difference (A.18), we conclude

$$\dot{\delta} = \frac{2e}{\hbar}V = \frac{2\pi}{\Phi_0}V \tag{A.25}$$

A.2.3 Junction Energy

Given the Voltage-phase relation (A.25) and the current-phase relation (A.20), integrating the product of current and Voltage in time will give us the energy stored in the magnetic field around a Josephson junction as it acts as a non-linear inductor:

$$H_J = \int dt\ IV = \frac{\Phi_0 I_c}{2\pi}\int dt\ \dot{\delta}\sin\delta = -\frac{\Phi_0 I_c}{2\pi}\cos\delta = -E_J\cos\delta \tag{A.26}$$

A.3 SQUID Loops

Consider two Josephson junctions in parallel.

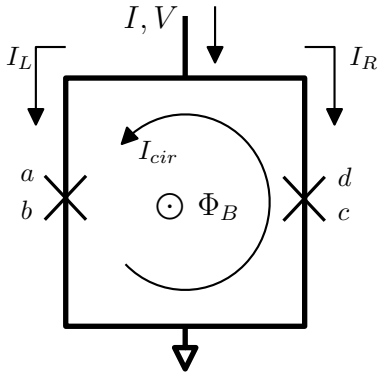

$$\delta_L = \theta_a - \theta_b + \frac{2e}{\hbar}\int_b^a \mathbf{A}\cdot d\mathbf{l}$$
$$\delta_R = \theta_d - \theta_c + \frac{2e}{\hbar}\int_c^d \mathbf{A}\cdot d\mathbf{l}$$
$$I_L = \frac{I}{2} + I_{cir} = I_c\sin\delta_L$$
$$I_R = \frac{I}{2} - I_{cir} = I_c\sin\delta_R$$

Figure A.2: A SQUID Loop

A.3.1 Flux Quantization

If we allow ourselves to treat the SQUID loop as constructed from a bulk superconductor by assuming weak magnetic fields, then we may assume that $\mathbf{J} = 0$ in the superconducting regions of the loop. By (A.16) then, we have

$$\nabla\theta = -\frac{2e}{\hbar}\mathbf{A} \tag{A.27}$$

for all regions excluding the junctions. We make use of the constraint that a closed path integral of $\nabla\theta$ must evaluate to an integer multiple of 2π, and take such a path integral around the SQUID loop:

$$\oint_C d\vec{l}\cdot(\nabla\theta) = \delta_R - \delta_L - \frac{2e}{\hbar}\oint_C d\mathbf{l}\cdot\mathbf{A} = 2\pi n \tag{A.28}$$

By Stokes' theorem,

$$\oint_C d\mathbf{l}\cdot\mathbf{A} = \iint_S d\mathbf{S}\cdot(\nabla\times\mathbf{A}) = \iint_S d\mathbf{S}\cdot\mathbf{B} = \Phi_B \tag{A.29}$$

Thus

$$\delta_R - \delta_L = \frac{2e}{\hbar}\Phi_B + 2\pi n = 2\pi(\frac{\Phi_B}{\Phi_0} + n) \tag{A.30}$$

When junctions in a superconducting loop do not exist, the left side of the equation is 0, and Φ_B is constrained to be an integer multiple of Φ_0.

When junctions do exist, we observe that Φ_B is permitted to be any value, and that the left side of the equation is constrained by the application of an external magnetic flux bias with a period of Φ_0. It is for this reason that SQUID loops are capable of being used as extremely sensitive magnetometers – very small external magnetic fields directly control the SQUID Hamiltonian:

A.3.2 SQUID Hamiltonian

For simplicity, let us assume that both junctions in a SQUID loop are identical. The asymmetric case is treated by Koch et al.[6], but the functional form of the result is equivalent. If we also allow ourselves to ignore the self-inductance of the SQUID loop, such that Φ_B is equal to an exterior, applied flux bias, then we see from (A.26) that the Hamiltonian for the SQUID loop is

$$H = -E_J\Big[\cos\delta_L + \cos\delta_R\Big] \tag{A.31}$$

By the relation between the two phases (A.30), this becomes

$$H = -E_J\Big[\cos\delta_L + \cos\left(\delta_L + 2\pi\frac{\Phi_B}{\Phi_0}\right)\Big] \tag{A.32}$$

$$= -2E_J\cos\left(\frac{\pi\Phi_B}{\Phi_0}\right)\cos\left(\delta_L + \frac{\pi\Phi_B}{\Phi_0}\right) \tag{A.33}$$

If we assume that Φ_B is effectively constant over the timescale of phase evolution (qubit oscillation), then we may introduce the change of variables

$$\delta_s \equiv \delta_L + \frac{\pi\Phi_B}{\Phi_0} \quad ; \quad \dot{\delta}_s = \dot{\delta}_L \tag{A.34}$$

This change of variables preserves the Voltage-phase relation (A.25). While it changes the form of the current phase relation (A.20), we have the convenience of being able to characterize a superconducting qubit without appealing to the current through SQUID loop for our purposes. With this change of variables, we see that we may write the Hamiltonian for the SQUID loop as

$$H = -E_s(\Phi_B)\cos\left(\delta_s\right) \quad ; \quad E_s(\Phi_B) = 2E_J\cos\left(\frac{\pi\Phi_B}{\Phi_0}\right) \tag{A.35}$$

Where

$$\dot{\delta}_s = \frac{2\pi}{\Phi_0} V$$

Appendix B

The Quantum Bit (Qubit)

B.1 General Qubits

B.1.1 Representation (Bloch Sphere)

While we have given a general representation for the pure state of a single qubit (1.1), it is worth noting that only the relative complex phase between the 0 and 1 states matters for the dynamics of one qubit. This allows us to rewrite $|\psi\rangle$ with only two degrees of freedom:

$$|\psi\rangle = \cos\frac{\theta}{2}|0\rangle + \sin\frac{\theta}{2}e^{i\phi}|1\rangle \tag{B.1}$$

Where $0 \leq \theta \leq \pi$ and $0 \leq \phi \leq 2\pi$ describe a point on the surface of a sphere named after Felix Bloch.

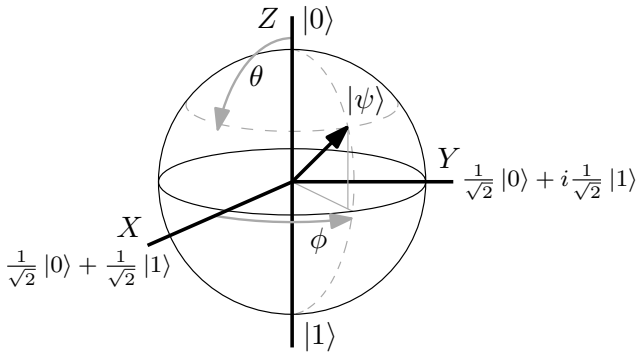

Figure B.1: The Bloch Sphere

$$\boldsymbol{\psi} = \hat{\mathbf{z}}\cos\theta + \hat{\mathbf{y}}\sin\theta\sin\phi + \hat{\mathbf{x}}\sin\theta\cos\phi \tag{B.2}$$

That the ground state is plotted at the North pole of the sphere seems backwards, but this is done for the sake of increased visibility of the Bloch vector near the ground state as opposed to the excited state.

A pure state may also be mapped onto the Bloch sphere by appealing to the density matrix. For a pure state, the density matrix is simply

$$\hat{\rho} = |\psi\rangle\langle\psi| \tag{B.3}$$

Substituting (B.1) into the definition for the density matrix, we use the basis $|0\rangle = \left(\begin{smallmatrix}1\\0\end{smallmatrix}\right)$, $|1\rangle = \left(\begin{smallmatrix}0\\1\end{smallmatrix}\right)$ to write

$$\hat{\rho} = \begin{pmatrix} \cos^2\frac{\theta}{2} & e^{-i\phi}\cos\frac{\theta}{2}\sin\frac{\theta}{2} \\ e^{i\phi}\cos\frac{\theta}{2}\sin\frac{\theta}{2} & \sin^2\frac{\theta}{2} \end{pmatrix} = \frac{1}{2}\begin{pmatrix} 1+\cos\theta & e^{-i\phi}\sin\theta \\ e^{i\phi}\sin\theta & 1-\cos\theta \end{pmatrix} \tag{B.4}$$

Referencing the basis formed by the Pauli matrices –

$$\hat{I} = \begin{pmatrix} 1 & 0 \\ 0 & 1 \end{pmatrix} \qquad \hat{\sigma}_x = \begin{pmatrix} 0 & 1 \\ 1 & 0 \end{pmatrix} \qquad \hat{\sigma}_y = \begin{pmatrix} 0 & -i \\ i & 0 \end{pmatrix} \qquad \hat{\sigma}_z = \begin{pmatrix} 1 & 0 \\ 0 & -1 \end{pmatrix} \tag{B.5}$$

we see that the density matrix may be expanded as

$$\hat{\rho} = \frac{1}{2}(\hat{I} + \hat{\sigma}_z \cos\theta + \hat{\sigma}_y \sin\theta \sin\phi + \hat{\sigma}_x \sin\theta \cos\phi) \tag{B.6}$$

Projecting the density matrix onto the space of the Bloch sphere according to

$$\boldsymbol{\rho} \equiv \rho_x \hat{\mathbf{x}} + \rho_y \hat{\mathbf{y}} + \rho_z \hat{\mathbf{z}} \quad ; \quad \hat{\rho} = \rho_0 \hat{I} + \rho_x \hat{\sigma}_X + \rho_y \hat{\sigma}_y + \rho_z \hat{\sigma}_z \tag{B.7}$$

we see that the vector is parallel to the Bloch sphere representation of $|\psi\rangle$ itself:

$$\boldsymbol{\rho} = \frac{1}{2}\boldsymbol{\psi} \tag{B.8}$$

B.1.2 Dynamics (Rotation)

This Bloch sphere representation of operators in the Pauli matrix basis is useful, because this allows us to map the Hamiltonian onto the Bloch sphere as well.

$$\mathbf{H} \equiv H_x \hat{\mathbf{x}} + H_y \hat{\mathbf{y}} + H_z \hat{\mathbf{z}} \quad ; \quad \hat{H} = H_x \hat{\sigma}_z + H_y \hat{\sigma}_y + H_z \hat{\sigma}_x \tag{B.9}$$

Appealing to the Liouville – von Neumann equation,

$$i\hbar \frac{\partial \hat{\rho}}{\partial t} = [\hat{H}, \hat{\rho}] \tag{B.10}$$

and the commutation relation between the Pauli matrices,

$$[\sigma_a, \sigma_b] = 2i\varepsilon_{abc}\, \sigma_c \tag{B.11}$$

we may view the Hamiltonian as an instantaneous rotation axis about which the qubit state precesses on the Bloch sphere.

$$\dot{\boldsymbol{\rho}} = \frac{1}{\hbar}(\mathbf{H} \times \boldsymbol{\rho}) \implies \dot{\boldsymbol{\psi}} = \frac{1}{\hbar}(\mathbf{H} \times \boldsymbol{\psi}) \tag{B.12}$$

This is functionally equivalent to Larmor precession.

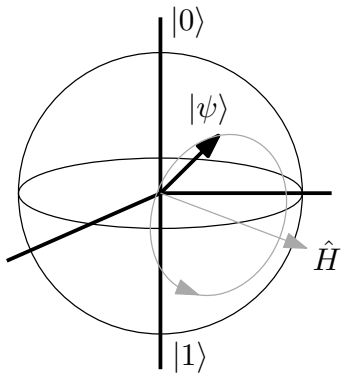

Figure B.2: Qubit Rotation

B.1.3 The Rotating Frame

Without any external fields, the qubit precesses about a Hamiltonian that is intrinsic to the two-level system (i.e. $|1\rangle$ is a higher-energy state than $|0\rangle$, and the $|1\rangle$ component of a Bloch state will lose phase relative to the $|0\rangle$ component at a rate proportional to the energy gap). The frequency of this precession is given by

$$f_{10} = \frac{E_1 - E_0}{2\pi\hbar} \equiv \frac{\omega_q}{2\pi} \tag{B.13}$$

and the Hamiltonian of the qubit in the absence of external fields may be written

$$\begin{pmatrix} -\hbar\omega_q/2 & 0 \\ 0 & \hbar\omega_q/2 \end{pmatrix} \tag{B.14}$$

This intrinsic Hamiltonian is always present, although we will see in the next section that f_{10} is tunable for some systems. Because all points on the Bloch sphere regress in phase (precess clockwise) together at a constant rate, it becomes useful to view the Bloch sphere in a rotating frame, where the effective dynamics of the natural qubit Hamiltonian are nullified and $\boldsymbol{\psi}$ remains static without an external field.

It is in this rotating frame that we wish to introduce externally-applied terms to the Hamiltonian which induce rotations about a fixed axis. Because the axis must be constant in the rotating frame, we must actually apply a Hamiltonian to the qubit which also regresses in phase on the Bloch sphere at an angular frequency ω_q.

Let us motivate the formula for the necessary change of basis: Consider an operator that rotates a state counter-clockwise around the Bloch sphere by an angle $\omega_q t$:

$$\hat{R} = \begin{pmatrix} e^{-i\omega_q t/2} & 0 \\ 0 & e^{i\omega_q t/2} \end{pmatrix} \tag{B.15}$$

Consider a state $|\psi\rangle$ in the lab frame which evolves by Schrödinger's equation in accordance with the Hamiltonian $\hat{H}$. In the rotating frame, the description of the same state $|\psi\rangle_{rot}$ appears to advance by $\omega_q t$ counter-clockwise relative to the lab frame description and to evolve according to the Hamiltonian $\hat{H}_{rot}$.

$$\hat{H}\,|\psi\rangle = i\hbar\partial_t(|\psi\rangle) \quad ; \quad |\psi\rangle_{rot} = \hat{R}\,|\psi\rangle \quad ; \quad \hat{H}_{rot}\,|\psi\rangle_{rot} = i\hbar\partial_t(|\psi\rangle_{rot}) \tag{B.16}$$

Joining these equations, we find

$$\begin{aligned}
\hat{H}_{rot}\left|\psi\right\rangle_{rot} &= i\hbar\partial_t(\hat{R}\left|\psi\right\rangle) \\
&= i\hbar\left[\dot{\hat{R}}\left|\psi\right\rangle + \hat{R}|\dot{\psi}\rangle\right] \\
&= i\hbar\dot{\hat{R}}\left|\psi\right\rangle + \hat{R}\hat{H}\left|\psi\right\rangle \\
&= i\hbar\dot{\hat{R}}\hat{R}^\dagger\left|\psi\right\rangle_{rot} + \hat{R}\hat{H}\hat{R}^\dagger\left|\psi\right\rangle_{rot} \\
\implies \hat{H}_{rot} &= i\hbar\dot{\hat{R}}\hat{R}^\dagger + \hat{R}\hat{H}\hat{R}^\dagger
\end{aligned} \tag{B.17}$$

Substituting $\hat{R}$, we conclude that for a general Hamiltonian,

$$\hat{H} = \begin{pmatrix} a & b \\ c & d \end{pmatrix} \implies \hat{H}_{rot} = \begin{pmatrix} a + \hbar\omega_q/2 & b(e^{-i\omega_q t}) \\ c(e^{i\omega_q t}) & d - \hbar\omega_q/2 \end{pmatrix} \tag{B.18}$$

For the case of the intrinsic Hamiltonian of the qubit, $\hat{H}_{rot}$ is identically 0, as desired.

B.2 Superconducting Qubits (The Transmon)

Although different superconducting qubit constructions are possible – utilizing different dynamical variables as good quantum numbers – we will focus our discussion on the transmon, which is a variation of the superconducting charge qubit. Most of our discussion is readily adapted to other architectures.

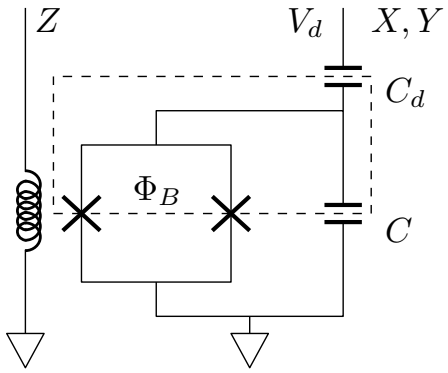

Figure B.3: A Transmon Qubit

The transmon qubit is constructed from a superconducting quantum interference device (SQUID) placed in parallel with a capacitor and capacitively coupled to a drive voltage (the XY line). The energy of the SQUID is tunable by the application of an external flux, via inductive coupling to the Z line.

We will show that the amount of electric charge contained on the superconducting island (sometimes called a "Cooper pair box") demarcated by the dashed line in the figure above behaves according to the dynamics of an anharmonic LC oscillator and forms our qubit.

B.2.1 Hamiltonian

As shown in A.3.2, by equation (A.35) the energy of a SQUID loop may be written like flux-tunable junction energy:

$$-E_s(\Phi_B)\cos\delta \tag{B.19}$$

where E_s is the maximum unbiased energy of the SQUID, δ is the effective phase difference across it, and where we have ignored self-inductance to treat Φ_B as a static, external flux bias applied through inductive coupling to the Z control line.

The energy of the two capacitors may be written

$$\frac{1}{2}C_d(V_d - V_s)^2 + \frac{1}{2}CV_s^2 \tag{B.20}$$

Recalling the Voltage-phase Josephson relation (A.25)

$$V_s = \frac{\Phi_0}{2\pi}\dot{\delta} \tag{B.21}$$

we identify terms with δ as potential energy and terms with $\dot{\delta}$ as kinetic energy. Neglecting terms with no dependence on δ, we may write the Lagrangian for the system as

$$\mathcal{L} = \frac{C_\Sigma}{2}\left(\frac{\Phi_0\dot{\delta}}{2\pi}\right)^2 - C_dV_d\left(\frac{\Phi_0\dot{\delta}}{2\pi}\right) + E_s(\Phi_B)\cos\delta \tag{B.22}$$

The canonical momentum of the system is the charge located on the superconducting island:

$$\begin{aligned}\frac{\partial\mathcal{L}}{\partial\dot{\delta}} &= \frac{{\Phi_0}^2}{2\pi}C_\Sigma\,\dot{\delta} - \frac{\Phi_0}{2\pi}C_dV_d \\ &= \frac{\Phi_0}{2\pi}\left[CV_s + C_d(V_s - V_d)\right] \\ &= \frac{\Phi_0}{2\pi}Q\end{aligned} \tag{B.23}$$

from which we extract the Voltage relation

$$\frac{\Phi_0}{2\pi}\dot{\delta} = \frac{Q + C_dV_d}{C_\Sigma} \tag{B.24}$$

Substituting Q into the Lagrangian according to (B.24) and again neglecting constant terms, we have

$$\mathcal{L} = \frac{Q^2}{2C_\Sigma} + E_s(\Phi_B)\cos\delta \tag{B.25}$$

We apply the standard Legendre transformation

$$H = \frac{\partial \mathcal{L}}{\partial \dot{\delta}} \dot{\delta} - \mathcal{L} \tag{B.26}$$

to obtain

$$H = \frac{Q^2}{2C_\Sigma} - E_s(\Phi_B)\cos\delta + \frac{C_d}{C_\Sigma} Q V_d \tag{B.27}$$

This system is a driven anharmonic oscillator.

B.2.2 First Quantization

While qubit anharmonicity is desired to avoid having equal energy separation between the states of the qubit (and thus possible two-photon transitions to the second excited state), we will not concern ourselves with the two-level dynamics of the system here. We thus assume low energy states and Taylor expand in δ to obtain a two-level Hamiltonian:

$$\hat{H} = \frac{\hat{Q}^2}{2C_\Sigma} + \frac{\hat{\delta}^2}{2} E_s(\Phi_B) + \frac{C_d}{C_\Sigma} \hat{Q} V_d \tag{B.28}$$

The state of the qubit may be described by a wavefunction in δ-space. In this picture, we have that

$$\hat{Q} \equiv -i\hbar \frac{2\pi}{\Phi_0} \partial_\delta = -2ie\partial_\delta \quad ; \quad [\hat{\delta}, \hat{Q}] = 2ie \tag{B.29}$$

We reference Appendix B in the thesis by D. Sank [9] to introduce the ladder operator

$$\hat{a} = \frac{1}{2\sqrt{e}} \left[\Big(C_\Sigma E_s(\Phi_B) \Big)^{1/4} \hat{\delta} + i \Big(C_\Sigma E_s(\Phi_B) \Big)^{-1/4} \hat{Q} \right] \tag{B.30}$$

We may thus rewrite the Hamiltonian

$$\hat{H} = \hbar\omega(\Phi_B) \left(\hat{a}^\dagger \hat{a} + \frac{1}{2} \right) - ig(\Phi_B) \Big(\hat{a} - \hat{a}^\dagger \Big) V_d \tag{B.31}$$

where

$$\omega(\Phi_B) = \frac{2\pi}{\Phi_0}\sqrt{\frac{E_s(\Phi_B)}{C_\Sigma}} \quad ; \quad g(\Phi_B) \equiv \frac{C_d\sqrt{e}\Big(E_s(\Phi_B)\Big)^{(1/4)}}{(C_\Sigma)^{(3/4)}} \tag{B.32}$$

We note as an aside that g has units of charge. Referencing (A.35), we note that the dependence of g on Φ_B looks like $\cos^{(\frac{1}{4})}$ and is approximately constant away from $\Phi_B/\Phi_0 = \pm\frac{1}{2}$. For small flux bias, we conclude that the effect on X and Y rotations during a Z rotation will be small.

As an additional note, the tuning of the anharmonicity and relative width of the δ and Q-space waveforms is addressed by Koch et al,[6] using the ratios of the variables we have presented. This work introduced the transmon qubit.

Having successfully written the Hamiltonian in terms of ladder operators, we may thus express the Hamiltonian in matrix form in the computational basis of energy eigenstates according to

$$|0\rangle = \begin{pmatrix}1\\0\end{pmatrix} \qquad |1\rangle = \begin{pmatrix}0\\1\end{pmatrix} \qquad \hat{a} = \begin{pmatrix}0 & 1\\0 & 0\end{pmatrix} \qquad \hat{a}^\dagger = \begin{pmatrix}0 & 0\\1 & 0\end{pmatrix} \tag{B.33}$$

Subtracting out the identity component from the Hamiltonian, we are left with

$$\hat{H} = \begin{pmatrix}-\hbar\omega/2 & -igV_d\\ igV_d & \hbar\omega/2\end{pmatrix} \tag{B.34}$$

B.2.3 Qubit Driving

That the qubit frequency is tunable by Φ_B leads to the possibility of rotations about the Z-axis in a straight-forward way – temporarily increasing or decreasing the qubit frequency relative to some standard ω_q will cause a net loss or gain of phase of the state $|\psi\rangle$ as observed in the ω_q frame. We will thus focus on X and Y rotations in the rotating frame of frequency $\omega(\Phi_B)$, whatever it may be.

In this frame, the transmon Hamiltonian (B.34) is transformed according to (B.18) to become

$$\hat{H}_{rot} = \begin{pmatrix} 0 & gV_d e^{-i\omega t} \\ gV_d e^{i\omega t} & 0 \end{pmatrix} \tag{B.35}$$

Decomposing the Hamiltonian according to (B.9), we have

$$\hat{H}_{rot} = gV_d\Big(-\sin(\omega t)\hat{\sigma}_x + \cos(\omega t)\hat{\sigma}_y \Big) \tag{B.36}$$

Let us express an arbitrary drive voltage in the form

$$V_d = Y(t)\cos(\omega t) - X(t)\sin(\omega t) \tag{B.37}$$

we expand

$$\hat{H}_{rot} = \frac{g}{2}\left[\begin{array}{r} \hat{\sigma}_x\Big[X(t)\Big(1-\cos(2\omega t)\Big) - Y(t)\Big(\sin(2\omega t)\Big)\Big] \\ +\hat{\sigma}_y\Big[Y(t)\Big(1+\cos(2\omega t)\Big) - X(t)\Big(\sin(2\omega t)\Big)\Big] \end{array}\right] \tag{B.38}$$

The high-frequency terms introduce oscillating signals to the control of the instantaneous axis of rotation in a way that maps perfectly to our discussion of sidebands in Chapter 2. We see that (B.38) maps perfectly to equations (2.39) and (2.40) when $s = 1$ and $\xi + \eta = \pi$.

We approximate the error we anticipate due to sidebands in Section 3.2, with the corresponding error mapped in Fig 3.3. For qubit frequencies greater than 5 GHz and gate times greater than 10 ns, we anticipate errors on the order of 10^{-8}, and are justified in neglecting these high-frequency terms.

As such, we are left with a Bloch sphere projection of the Hamiltonian (B.9) in the rotating frame given by

$$\mathbf{H}_{rot} \approx \frac{g}{2}\Big(X(t)\hat{x} + Y(t)\hat{y}\Big) \tag{B.39}$$

and we are able to match drive Voltages of the form (B.37) to instantaneous rotation axes on the Bloch sphere in the rotating frame of the qubit.

Bibliography

[1] Austin G. Fowler, Matteo Mariantoni, John M. Martinis, and Andrew N. Cleland. Surface codes: Towards practical large-scale quantum computation. *Phys. Rev. A*, 86:032324, Sep 2012.

[2] John M. Martinis and Kevin Osborne. Superconducting Qubits and the Physics of Josephson Junctions. In *Les Houches*, volume 79, pages 1–608. École d' été de Physique des Houches Session LXXIX, 2004.

[3] J. Kelly, R. Barends, A. G. Fowler, A. Megrant, E. Jeffrey, T. C. White, D. Sank, J. Y. Mutus, B. Campbell, Yu Chen, Z. Chen, B. Chiaro, A. Dunsworth, I.andC. Hoi, C. Neill, P. J. J. O/'Malley, C. Quintana, P. Roushan, A. Vainsencher, J. Wenner, A. N. Cleland, and John M. Martinis. State preservation by repetitive error detection in a superconducting quantum circuit. *Nature*, 519:66–69, Apr 2015.

[4] Julian Kelly. *Single Qubit Bootstrapping and Gate Calibration.* B.S. Thesis, UC Santa Barbara, 2010.

[5] E. Knill, D. Leibfried, R. Reichle, J. Britton, R. B. Blakestad, J. D. Jost, C. Langer, R. Ozeri, S. Seidelin, and D. J. Wineland. Randomized benchmarking of quantum gates. *Phys. Rev. A*, 77:012307, Jan 2008.

[6] Jens Koch, Terri M. Yu, Jay Gambetta, A. A. Houck, D. I. Schuster, J. Majer, Alexandre Blais, M. H. Devoret, S. M. Girvin, and R. J. Schoelkopf. Charge-insensitive qubit design derived from the cooper pair box. *Phys. Rev. A*, 76:042319, Oct 2007.

[7] Ferenc Marki and Christopher Marki. Mixer basics primer. Technical report, Marki Microwave.

[8] Michael A. Nielsen and Isaac L. Chuang. *Quantum Computation and Quantum Information: 10th Anniversary Edition.* Cambridge University Press, New York, NY, USA, 10th edition, 2011.

[9] Daniel Sank. *Fast, Accurate State Measurement in Superconducting Qubits.* PhD dissertation, UC Santa Barbara, 2014.